Normalization-free Chipless RFIDs by using Dual Polarized Interrogation

Filippo Costa, *Member, IEEE*, Simone Genovesi, *Member, IEEE*, Agostino Monorchio, *Fellow, IEEE*

***Abstract*—A reliable encoding/detection scheme for chipless Radio Frequency Identification (RFID) tags, free from any normalization procedure, is presented. The key strategy of the present approach consists in storing the information in the difference between vertically and horizontally polarized reflection coefficients of a completely passive tag. The measured reflection coefficients are preemptively filtered in the time domain to remove most of harmful effects due to the antenna coupling and environment multipath and finally they are subtracted to obtain the differential response. A couple of chipless tag configurations suitable for providing the desired spectral response are presented. The resonators consist of an Artificial Impedance Surface (AIS) comprising either concentric rectangular loop resonators or square loop resonators loaded with stubs. The presented approach is experimentally verified in a non-anechoic environment and its robustness is proved. This calibration-free approach could pave the way to practical applicability of chipless RFID tags in realistic scenarios with unknown response.**

***Index Terms*— Artificial Impedance Surface (AIS), Chipless RFID, Frequency Selective Surfaces (FSS), Metamaterials, Radio Frequency Identification (RFID).**

I. INTRODUCTION

The main hurdle towards the applicability of Radio Frequency Identification (RFID) technology in place of conventional barcodes is the cost of the tags that, even if has considerably dropped in the last decade, still remains too high [1]. Identification or tracking of objects by using radio frequencies may provide interesting advantages with respect to barcode, such as the non-line of sight and the quickness of the reading procedure. However, the advantages are often not sufficient to justify big investments of a company to setting up a new tracking technology. A solution to overcome this problem could be the use of an RF barcode that is eventually low-cost as the optical barcode but still preserves some of the advantages guaranteed by the use of radio frequencies (*e.g.* quick reading of tags, correct working even in absence of optical visibility). Clearly, the removal of the IC transforms the tag in a completely passive scatter having some drawbacks with respect to conventional chip-equipped devices. Indeed, it cannot be reprogrammable and it often requires ultra-wide band interrogation systems [2]. However, the RF barcode has also some advantages such as a much lower cost, absence of a minimum power threshold for activating the tag response and usability in harsh environments. The potentialities in terms of limited cost make chipless technology a good candidate to replace barcode and magnetic cards in several realistic scenarios.

Chipless RFIDs can be divided into two main categories: those that store information in the time domain (TD) and those that does it in the frequency domain (FD). The most popular TD tag is the one based on surface acoustic wave (SAW) [3]. However, it is not sufficiently cheap compared to standard RFID tags. Time-domain based chipless tags employing printed delay lines have a limited number of encoded bits per area [4]–[6]. The FD class of chipless tags comprises spectral signature-based tags. These tags encode data into the spectrum using resonant structures associating a bit with the presence or absence of a resonant peak at a predetermined frequency in the spectrum. These tags are promising for their potentially large data storage and low manufacturing costs. So far, a number of chipless tag configurations have been proposed [2], [7]–[9]. FD tags can be partitioned into two main groups. Those which receive, filter and retransmit a interrogating signal through orthogonally polarized antennas with a multi-band resonator in between [10] and those which employ a set of multi-frequency scattering resonators [9].

Beyond the specific configuration adopted to encode the information, the main limitation of chipless technology is that the tag detection requires a calibration procedure based on two or three independent measurements performed on the same scenario (tag and background and eventually ground plane). Even if in a laboratory environment this procedure is feasible, this is not an option in a real scenario. A normalization is feasible only in a few situations where it is possible to store the background response in advance. For example, the case of a conveyor belt or those cases where a tag moves with respect to the interrogating antenna. However, in general, the absence of a reference makes the tag reading nearly unfeasible. In order to overcome this fundamental problem and pave the way to a realistic implementation of chipless technology in more complicate scenarios, we propose a new encoding/decoding scheme based on two simultaneous acquisitions along two orthogonal planes of incidence followed by post-processing combination of stored data. This approach can be carried out in a realistic scenario by using a reader with a dual-polarized antenna. Some preliminary results of the same method were presented in [11] where the idea of using a dual polarized interrogation was introduced. However, the reported experimental results were unprocessed and valid only for one-

Manuscript received March, 11th 2015.

F. Costa, S. Genovesi, and A. Monorchio are with Department of Information Engineering, University of Pisa, Via G. Caruso, 56122 - Pisa. E-mail: filippo.costa (simone.genovesi, a.monorchio)@iet.unipi.it

bit tags. Here a novel and reliable algorithm for post-processing measured data is introduced. Moreover, new tag configurations designed for the dual-polarized interrogation are described and experimentally tested. The paper is organized as follows. The encoding/decoding approach is introduced in Section II: Possible tag configurations able to provide the differential encoding scheme are described in Section III. In Section IV the proposed strategy is experimentally validated for several tag configurations. Section V is devoted to the description of the decision strategy whereas the following Section VI deals with the read range. Concluding remarks are drawn in Section VII.

II. ENCODING/DECODING PROCEDURE

The reading of chipless RFID tags requires, in most of practical scenarios, a normalization procedure based on the knowledge of the background response [7], [9], [10], [12]. The procedure allows removing mutual coupling effects between the two ports of the antenna and undesired reflections due to multipath propagation. This calibration can be easily applied in a controlled environment where the background response is characterized with a preliminary measure but it represents one of the main obstacles towards practical applicability of chipless technology.

In order to perform a calibration-free reading, three strategies are jointly adopted: dual polarization interrogation, time domain gating and free space antenna response subtraction.

The first necessary step is to encode the information in the difference between two responses such as, for instance, the reflection coefficient of the tag measured with respect vertical and horizontal polarizations. This is the key point since it allows encoding the information in a differential response instead of an absolute one. We remark that the coding with two polarizations is not adopted to improve the coding capacity of the tag but to make the reading procedure more robust.

The second step consists of subtracting the reflection coefficients of the unloaded antenna (*i.e.* antenna operating in free space, not in the operative scenario) from the reflection coefficients measured in presence of the tag (*i.e.* antenna in operative scenario). The reason of this subtraction is that every dual-polarized antenna does not have the same reflection coefficient at port #1 and port #2 and hence s_{11} is different from s_{22}. Since the measured signals in presence of the tag are very small, the intrinsic difference between the two antenna ports could invalidate the decoding procedure. The unloaded reflection coefficients of the antenna are independent of the scenario and they are considered as known parameters.

The third step is the time domain gating which allows removing some of the harmful effects due to the antenna coupling and to the multipath phenomena. To perform this operation, the distance of the tag is estimated by tracking the the first structural RCS peak. Time gating is a quite standard technique for radar signal processing [13], microwave imaging [14] electromagnetic measurement [15] or even chipless RFID [16]. However, it has to be pointed out that the sole use of dual polarization interrogation or time domain gating does not provide a sufficient intelligible signal at the receiver [17], [12].

The aforementioned differential coding of information can be achieved by designing a passive resonator characterized by a multi-resonant frequency response for each of the two orthogonal polarizations. By tailoring the tags so that the spectral responses are slightly shifted, the received signals can be combined (summed or subtracted) to provide well recognizable high quality factor frequency peaks. The aforementioned multi-frequency responses can be obtained for example by employing either a rectangular loop resonator or a square loop resonator loaded with slightly different stubs along two planar orthogonal planar directions. The details about the adopted tag configurations are given in the next section. The steps followed to accomplish the proposed decoding procedure are summarized in the flowchart reported Fig. 1. Initially, the s_{11} and the s_{22} of the antenna are simultaneously measured in the operative scenario with the tag where s_{11} is to the vertical probing signal and s_{22} to the horizontal one. Next, the s_{11} and the s_{22} of the antennas measured in free space are subtracted to the aforementioned ones. These new signals, named *V(f)* and *H(f)* for convenience, are then post-processed. More in detail, they are anti-transformed in the time-domain and then filtered by using a window for removing most of the effects due to antenna coupling and multipath. The filtered responses are then transformed again into the frequency domain. The amplitude of the two signals is stored and converted in decibel. Finally, they are subtracted and a threshold decision scheme, based on the standard deviation of the differential signal within the expected frequency window, is adopted. A more advanced elaboration [18], [19] could be also employed at this stage to retrieve the encoded bits.

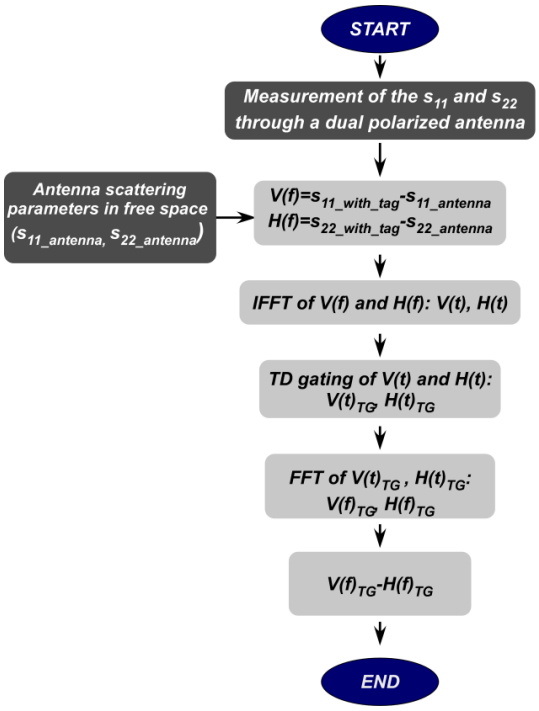

Fig. 1 – Flow-chart of the decoding procedure.

III. Dual Polarized Chipless Tag Configurations

The most important feature on which the proposed calibration scheme is the multi-resonant backscattering frequency response of the tags for the two orthogonal polarizations (vertical and horizontal). The two responses have to be slightly shifted in frequency domain in order to achieve very sharp peaks when the curves are subtracted in post-processing.

To achieve the desired frequency behavior, we have to introduce a certain asymmetry in the resonator. Among several possibilities, we have selected two promising geometries: the former is a rectangular loop that provides different resonant frequencies if the E-field is aligned to the longer or the shorter side of the loop. The latter is a square loop loaded with stubs of different length along the two main planar directions.

It is also desirable having a tag with a ground plane to reduce the sensitivity of the spectral response to the tagged object and eventually to the background. The selectivity of the frequency domain response is achieved by using resonators arranged in a periodic manner, *i.e.* Frequency Selective Surface (FSS) accommodated in the vicinity of a ground plane. The FSS and the ground plane forms an interference device with high spectral selectivity which will be referred as artificial impedance surface in the following. The resonant structure can provide both reflection and absorption while transmission coefficient is equal to zero because of the presence of ground plane. The AIS, differently from non-periodic configurations, can be rapidly analyzed as an infinite extent surface by using a Periodic Method of Moment (PMM) [20] or modeled though an equivalent circuit approach [21]. In this paper simulations are carried out by using an in-house developed PMM code [22]. This method uses the Electric Field Integral Equation (EFIE) formulation and the Floquet theory to simulate an infinite array of resonators. The advantage of this method with respect to commercial codes is that the computation time is very limited and the results are reliable. Clearly, in practice, the resonator has a finite dimension but the frequency response in terms of resonant peaks matches well with the measured results [9], [23].

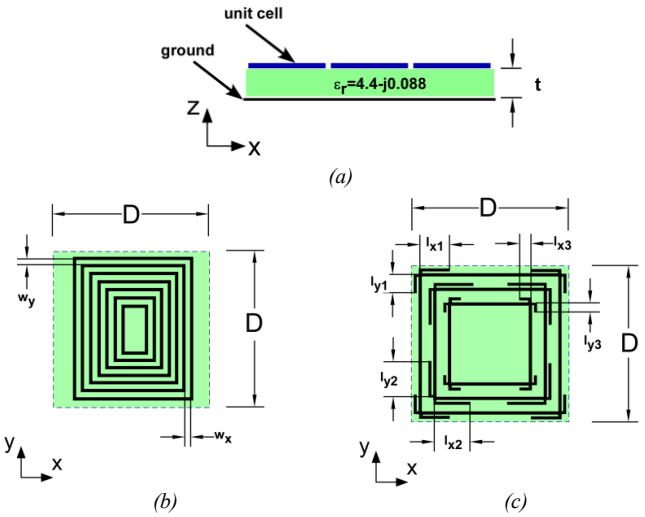

Fig. 2 – (a) Layout of the tag from a side view and geometry of the FSS unit cells of the periodic surface on top of the grounded dielectric slab: (b) several nested loops or (c) three loops loaded with stubs with a different length towards *x* and *y* direction.

A robust compact and versatile multi-resonant FSS configuration is offered by concentric loops [9], [24].

The first approach to design a tag with multi-resonant behavior, shifted for the two polarizations, is to stretch the loops towards one of the two planar axis obtaining a set of concentric rectangular loops. The layout of the proposed unit cell and the side view of the tag is reported in Fig. 2a and Fig. 2b. The degree of stretch, which means different gaps w_x and w_y along *x* and *y* directions, provides the amount of the shift achieved in the frequency domain between the two spectral responses. In this case, every resonant loop encodes a bit of information and the presence or the absence of the loop determine an amplitude modulation on a specific resonant band. The other possible configuration comprises square resonant loops loaded with stubs on the corners. The layout of the unit cell is displayed in Fig. 2c. The length of the stubs is different along *x* and *y* directions in order to provide the desired shifted frequency response. The use of stubs allows adopting a hybrid coding technique since resonant peaks can be easily moved by changing the length of the stubs [25]. In the latter case, the information coding is not binary but it can have a larger base which depends on the number of states of the loop [7]. The use of only three loops guarantees the absence of the coupling between the loop resonators thus providing the independence of all encoded states. By using the hybrid coding technique it is possible to encode almost 16 bits with three loops only [25]. The bit number could be, in principle, further increased (for instance by using fours loops) but there can be issues about coupling between loops. For the configuration including only rectangular loops, 10 bits can be easily encoded. By decreasing the width of each loops and the gaps between one loop and another, the number can be extended to 20 bits. The main limitation in this case is given by the precision of lithographic process, say 5 mils.

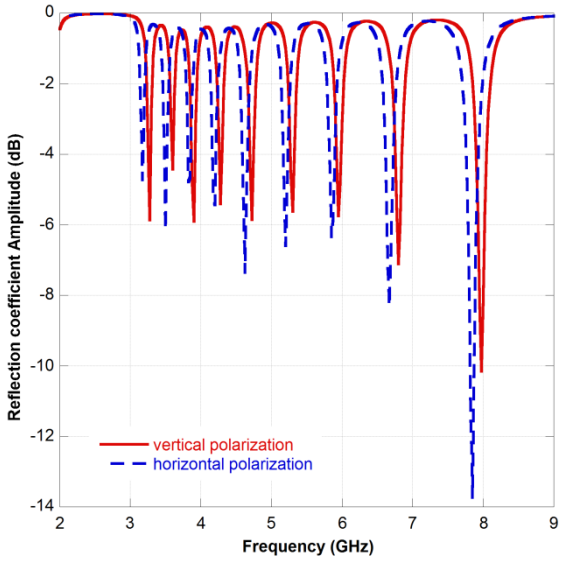

Fig. 3 - Amplitude reflection coefficient of a periodic artificial impedance surface comprising ten nested rectangular loops according to the unit cell design reported in Fig. 2b. The geometrical parameters are chosen as: w_x = 0.23 mm and w_y = 0.25 mm. The substrate is FR4 with ε_r = 4.4–j0.088. The unit cell periodicity *D* is equal to 15 mm.

Both of tag configurations perform deep absorptions over multiple resonance frequencies given that the substrate is characterized by a suitable amount of losses and the proper thickness [9], [26]. The reflection responses obtained with the proposed configurations are reported in Fig. 3 and in Fig. 4. In both cases, the unit cell periodicity D is equal to 15 mm. Each unit cell is discretized with a regular grid of 64×64 pixels leading to a pixel dimension of 0.234 mm, which is still well above the limit of precision of the standard photolithographic process. An FR4 substrate ($\varepsilon_r = 4.4 - j0.088$) is chosen for its low cost whereas the thickness of 1.6 mm is chosen to maximize the absorption at the resonances with this specific substrate.

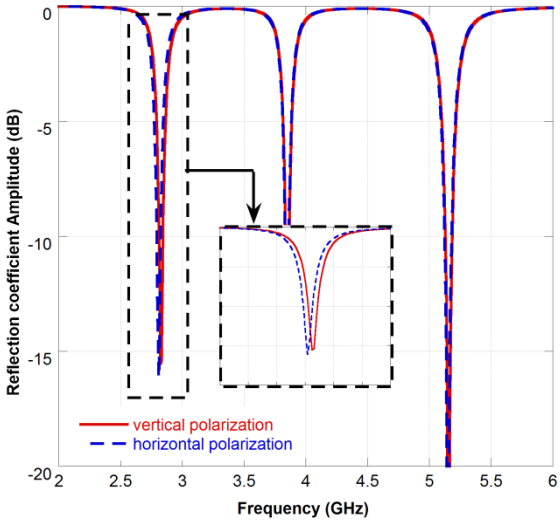

Fig. 4 - Amplitude reflection coefficient of an infinite array of a square loop loaded with different stubs printed on top of a grounded dielectric substrate. The reflection coefficient is computed at normal incidence for vertical and horizontal polarization. The substrate is FR4 with $\varepsilon_r = 4.4 - j0.088$.The unit cell periodicity D is equal to 15 mm.

In the case of the rectangular loop resonators, 10 bits are achieved by accommodating ten loops one inside another. The ten rectangular loops have $w_x = 0.23$ mm and $w_y = 0.25$ mm. In the case of the loaded loops, the width of the stubs is one pixel and their length is varied to change the encoded states. In both cases, well visible transitions in correspondence of every resonance frequency are obtained by subtracting the vertically and horizontally polarized reflection coefficients in a decibel scale. The smaller is the frequency shift between the response of the two polarizations, the higher is the Q-factor of the subtracted signals. As an example, the curve achieved by subtracting the vertical and horizontal polarized signal of Fig. 4 is reported in Fig. 5. The effect of the stub length on the resonant peaks is also highlighted by reporting two additional curves obtained by slightly varying the length of the x-directed stub associated to the external loop. As already pointed out, the shift of the resonance frequency can be exploited to enhance the number of encoding states.

The simulated results refer to infinite structures which is a good predictor of the spectral response of the truncated structure [9]. However, the response of the infinite periodic surface is not overlaid to the one of a finite surface in correspondence of the first resonance that is usually slightly shifted with respect to the measured data. This is due to the finiteness of the sample, which is not considered with the PMM code. However, this is not a real problem from a practical point of view since the precise position of the resonances can be found with measurements once for all.

When employed in an operative scenario, the periodic impedance surface is truncated to few unit cells and the number of unit cells can be suitably chosen to obtain the required level of Radar Cross Section (RCS), that is, the desired read range. Generally, a size of 2 x 2 unit cells, which corresponds to 30 x 30 mm^2, guarantees a sufficient level of scattered power to detect the tag at distances up to one meter.

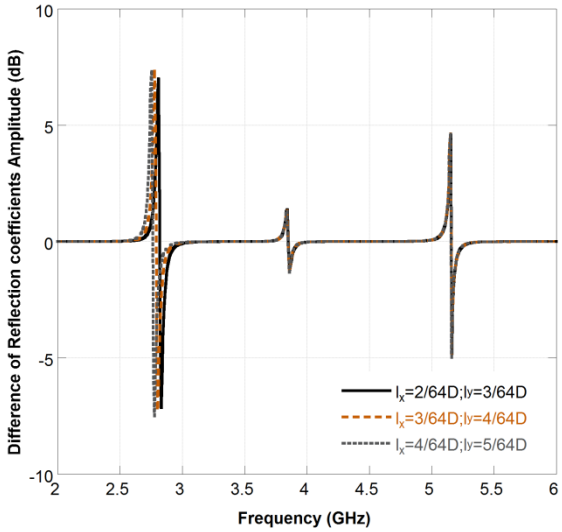

Fig. 5 - Amplitude difference between the reflection coefficients obtained for vertical and horizontal polarization. Geometrical parameters: $l_y = l_x+1$ with l_x equal to 2/64 D, 3/64 D, 4/64 D.

IV. Experimental Verification in a Non-Anechoic Environment

In order to verify the reliability of the proposed encoding scheme, several prototypes have been manufactured and measured. The prototypes have been fabricated by using a low-cost substrate, that is, 1.6 mm thick FR4. The response of the tag has been measured through a dual polarized horn antenna characterized by a gain of 8 dBi at 2 GHz and which increases up to 13.3 dBi at 8 GHz. The two channels, which are characterized by an isolation between -30 and -35 dB in the analyzed frequency range, are used to send the interrogating signals with vertical and horizontal polarization. The measurements have been performed in a non-anechoic environment, which is the microwave laboratory of the department of Information engineering of the University of Pisa, with the tag placed at a distance of 45 cm from the reading antenna. A picture of the employed setup is reported in Fig. 6.

As a test case, a chipless tag comprising 3 concentric loops loaded with stubs has been measured and decoded by using the classical calibration procedure and the proposed encoding/decoding scheme. The measured s_{11} and s_{22} of the interrogating antenna are reported in Fig. 7.

As it is evident, the recorded responses on the two channels, which are s_{11} and s_{22}, are quite different. This effect is mainly due to the intrinsic differences between the two ports of the antenna, not to the presence of the tag. However, since the s_{11}

and s_{22} of the antennas measured in free space are known, they can be subtracted from the collected measurements in presence of the tag. It has to be pointed out that this post-processing operation is completely independent of the scenario where the tag is embedded in. This preliminary subtraction allows removing the effect of the antenna matching and thus isolating only the signal contribution due to the tag and to the scenario. After that, the signals are transformed in time domain and windowed. The time gating allows removing some effects due the multipath and antenna coupling.

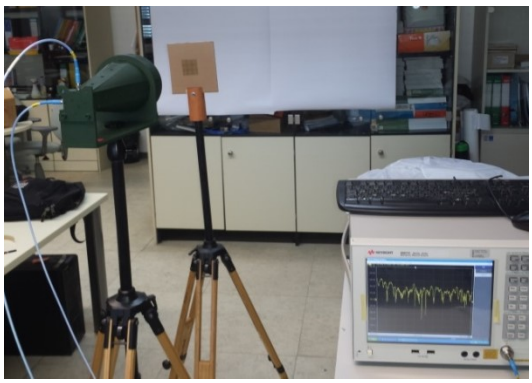

Fig. 6 – A picture of the experimental setup.

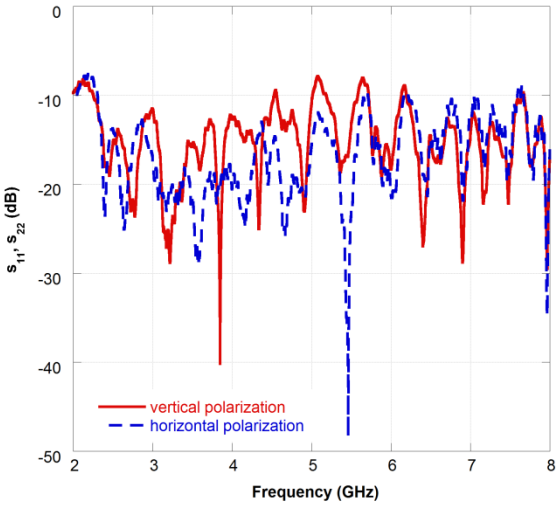

Fig. 7 - Measured s_{11} and s_{22} of the interrogating antenna with the chipless tag placed at 45 cm. S_{11} is for vertical polarization and s_{22} is for horizontal polarization.

The initial time step of the window applied to the received signals is related to the position of the tag. The first strong peak due to the structural component of the RCS allows identifying this parameter. The duration of the time gating is long enough to avoid any loss of information in the spectral domain. The TD window applied in this case is almost rectangular. There is a slight transition in the beginning of the window which makes the shape of the windows trapezoidal. We tried to use several windows (Hamming, Hanning, Triangular, Rectangular, Kayser, Blackmann-Harris etc.) but, in the end, the final results do not differ substantially provided that the three more important parameters (duration of the window, initial time, initial transition) are suitably set. The most important parameter is the length of the time window since it determines the bandwidth of the FD filter which convolutes the frequency domain response of the tag (the time domain multiplication can be seen as a convolution among the frequency domain response of the tag and the FFT transform of the window).

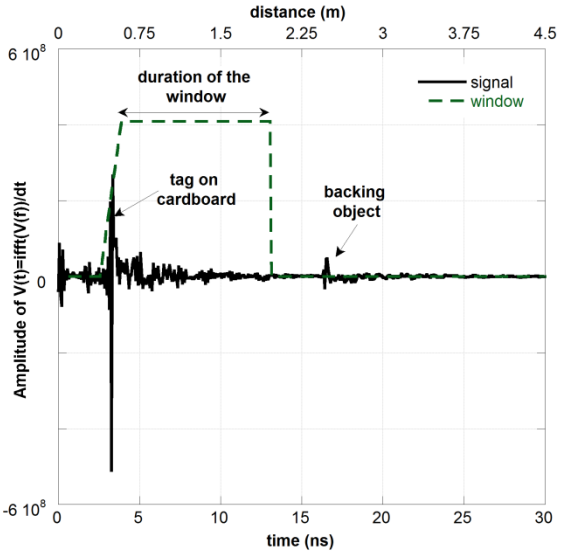

Fig. 8 - Time domain signal with the time window used to filter it. Time domain signal is obtained by applying the IFFT to the signal V(f) of Fig. 1.

The bandwidth of this filter, that is the FFT transform of the TD window, must be smaller or comparable to the bandwidth of the resonant peaks of the chipless RFID resonator. If this condition is not satisfied, the information associated to the RCS response will be lost in the convolution operation. For this reason, it has been estimated that the minimum duration of the window is 15 ns in this specific example where the bandwidth of the peaks is around 50 MHz.

The shape of the time domain window allows having a convolution frequency filter with higher or smaller rejection on side lobes. However, it has to be kept in mind that the time tapering increases the bandwidth of the main lobe for a certain fixed length of the window. The time window has to fulfill to two opposite requirements: it should be long enough to have a frequency response of the time window at least smaller than the frequency bandwidth of the resonant peaks but, at the same time, it should be short enough to filter out the RCS contributions of the objects close to the tag. Consequently, if there exist objects too close to the tag, the accuracy of the proposed technique decreases. The chosen trapezoidal window is a good choice since it allows to keep substantially unchanged that bandwidth of the main lobe of the filter in the frequency domain and to apply some tapering which reduce the contribution of other resonant peaks in the FD convolution. The precise initial time has been optimized empirically concluding that 1 ns before the presence of the strong peaks is a reasonable choice. The time domain signal and the filtering window are both reported in Fig. 8. The same signal is represented also in terms of distance by using $d = t \cdot c/2$, where c is the speed of light, t is the roundtrip time and d is the distance of the tag.

After the time gating, the two signal are transformed again into the frequency domain (Fig. 9). As it is apparent from Fig.

9, the two signals separately post-processed are still ambiguous. A number of resonant peaks can be observed, including the three searched ones, but it is complicate to separate the noise from the useful information. The amplitude reflection coefficients obtained for the two polarizations by using the classical normalization procedure [7], [9] are reported in Fig. 10 for comparison,. The standard procedure combines three measurements obtained in the same scenario (tag, ground plane of the same size of the tag and background measurement in absence of the tag) as follows:

$$s_{21}^{norm} = \frac{s_{21}^{tag} - s_{21}^{isol}}{s_{21}^{PEC} - s_{21}^{isol}}$$

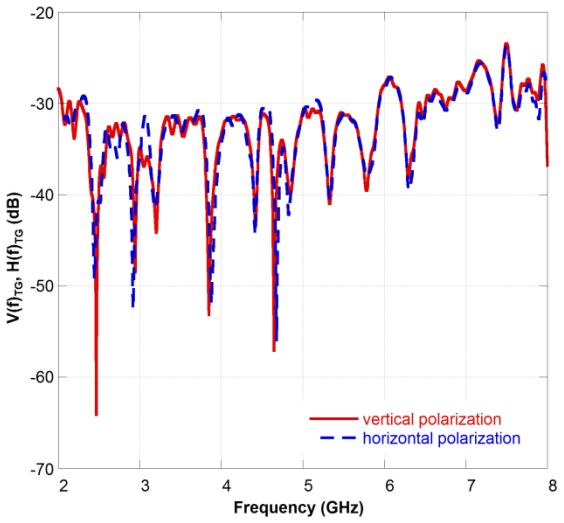

Fig. 9–Frequency domain signals for horizontal and vertical polarizations after time gating.

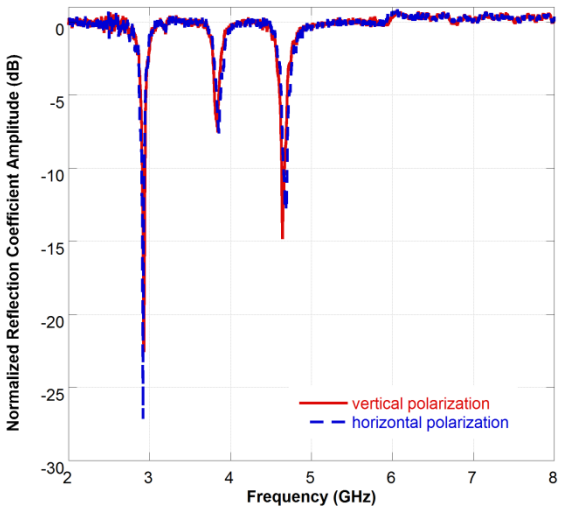

Fig. 10 - Reflection coefficient for vertical and horizontal polarizations obtained through the standard calibration procedure involving three simultaneous measurements (tag, ground plane of the same size of the tag and background measurement).

On the contrary, by using the approach here proposed, the bit sequence is decoded by using only a single measurement.

In order to improve the detectability of the received information, the amplitude of the two post-elaborated signals are subtracted in decibel scale. In this way, a much clearer curve is obtained. To facilitate the assessment of the derived result, the difference curve is compared, in Fig. 11, with the optimal result obtained by subtracting the calibrated signals of Fig. 10 as well as with the simulations of the infinite surface obtained with the PMM code. The curves agree well demonstrating that the use of polarization diversity results in a crucial improvement in the quality of the received signals and thus avoiding unpractical calibration procedures.

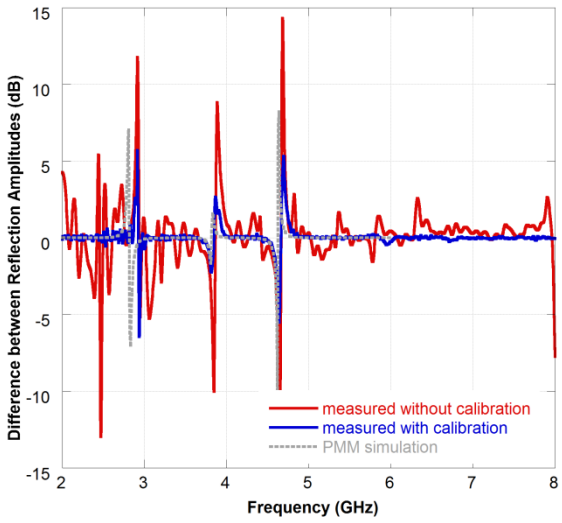

Fig. 11 - Measured amplitude difference between the vertically and horizontally polarized reflection coefficients of a three-bit tag. The result obtained by using the standard calibration procedure is compared with the one retrieved by avoiding the subtraction of the background and with simulated result. The simulated result obtained by using the PMM method is superimposed for comparison.

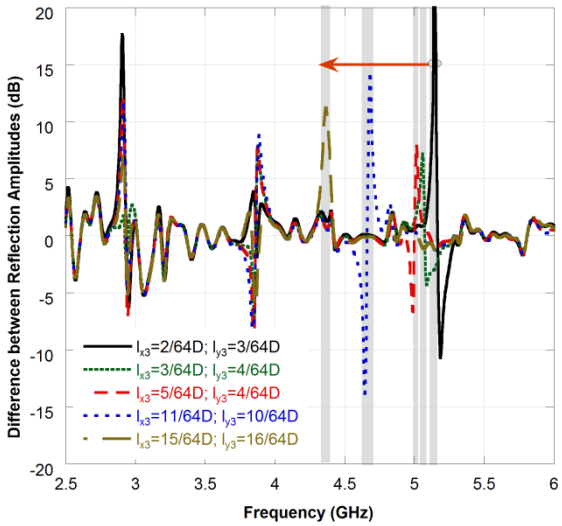

Fig. 12 - Measured amplitude difference for five different bit sequences obtained by progressively varying the length of the stubs of the third loop and imposing $l_{y3}=l_{x3}+1$ or $l_{x3}=l_{y3}+1$. The other stubs are fixed at the lowest length: $l_{x1}=l_{x2}=2/64D$, $l_{y1}=l_{y2}=3/64D$. Detection is performed by avoiding background subtraction.

To further assess the robustness of the presented method, a set of different tag configurations are measured and decoded. The reflection differences obtained by using the presented calibration-free method are reported in Fig. 12. Different stub lengths of the internal loop characterize the measured tags. As previously pointed out, the variation of the stubs length allows shifting the resonance peak associated to a specific loop and thus improving the coding capacity of the tag. It is evident that, in all cases, the present approach allows following the shift of the third peak. As shown in the figure, it is also possible to appreciate if the curves cross the zero from negative to positive (N→P) or from positive to negative (P→N), thus doubling the coding capacity. This behavior is simply obtained by using an *x*-oriented stub slightly longer than *y*-oriented one or vice versa. It is worth underlining that the other resonant peaks are unperturbed by the variation of the stub lengths associated to the third loop.

V. Decision Strategy

In order to define a decision strategy, some relevant parameters have been recorded on frequency windows around the expected resonance frequencies. The frequency windows, as highlighted in Fig. 12, are chosen with a bandwidth of 0.6% (f_0±0.3%) around each expected resonance frequency and the estimated parameters are the maximum absolute value, the standard deviation and the gradient of the curve. Some additional examples with the values of the aforementioned parameters are reported in Table 1 and Table 2. In those cases, stubs of the second and third loop are varied, respectively. The three resonance frequencies listed in the rows of the table are the ones expected for the stub configuration of the first column. As the stub lengths of the second and third loops are increased, the second resonant frequency (Table 1) and the third resonant frequency respectively (Table 2) are shifted. It is therefore expected to observe high standard deviation and a high maximum value within a new frequency window. Indeed, by observing for instance the values of standard deviation for the frequency of 5.16 GHz in Table 2, it is evident that the standard deviation of the curve drops from 12.9 to less than 0.89 when the stub is increased. Moreover, the maximum observed value decreases rapidly by increasing the stubs length. This means that both standard deviation and maximum value can be used to estimate the presence or absence of resonant peak in a certain narrowband frequency window. The standard deviation seems to be a better predictor for deciding about the presence or the absence of a peak within a certain frequency window with respect to the maximum value. The reason is that it is calculated by considering a set of frequency points instead of a single one.

The standard deviation of the curve is also a good predictor of the noise floor if estimated when the resonant peak is not present in a certain frequency window. For this reason, it can be used as a minimum threshold to overcome the decision for the presence of the resonant peak. Even very close frequency peaks can be distinguished with a threshold value of 2.5. The number of possible states has however to be decreased if possible intrinsic tolerances of the substrate permittivity are taken into account. For instance, if some variation of the dielectric permittivity among tags is expected, the frequency window band can be doubled and thus the number of states for each loop is halved. In the present case, the number of encoded bit would decrease from 15.8 to 12.8. Finally, it is pointed out that also phase responses can be exploited to cross-check the accuracy of the decoded bit sequence [27].

Table 1 – Estimation of the standard deviation (std) of the curve and its maximum value within the decision bandwidth f_0±0.3% while the stub of the second loop is varied. P → N stands for positive to negative slope of the curve.

	$l_{y1}=l_{x1}+1=3$ **$l_{y2}=l_{x2}+1=3$** $l_{y3}=l_{x3}+1=3$		$l_{y1}=l_{x1}+1=3$ **$l_{y2}=l_{x2}+1=4$** $l_{y3}=l_{x3}+1=3$		$l_{y1}=l_{x1}+1=3$ **$l_{y2}=l_{x2}+1=5$** $l_{y3}=l_{x3}+1=3$		$l_{y1}=l_{x1}+1=3$ **$l_{y2}=l_{x2}+1=11$** $l_{y3}=l_{x3}+1=3$		
f_0 (GHz)	**Std**	**Max**	**Std**	**Max**	**Std**	**Max**	**Std**	**Max**	**slope**
2.91	9.72	20.7	3.89	9.03	7.01	15.5	6.13	13.2	P→N
3.54	0.46	1.09	0.45	1.15	0.47	1.20	**7.07**	**12.4**	P→N
3.78	0.20	0.35	1.92	4.91	**3.39**	**6.59**	0.22	0.58	P→N
3.83	1.20	3.80	**4.68**	**7.41**	1.69	5.38	0.21	0.52	P→N
3.86	**3.19**	**4.08**	1.24	3.87	0.40	1.30	0.40	1.19	P→N
5.16	13.3	35.9	7.10	10.3	7.32	13.7	7.49	11.1	P→N

Table 2 - Estimation of the standard deviation (std) of the curve and its maximum value within the decision bandwidth f_0±0.3% while the stub of the third loop is varied. P → N stands for positive to negative slope of the curve.

	$l_{y1}=l_{x1}+1=3$ $l_{y2}=l_{x2}+1=3$ $l_{y3}=l_{x3}+1=3$		$l_{y1}=l_{x1}+1=3$ $l_{y2}=l_{x2}+1=4$ $l_{y3}=l_{x3}+1=4$		$l_{y1}=l_{x1}+1=3$ $l_{y2}=l_{x2}+1=5$ $l_{y3}=l_{x3}+1=5$		$l_{y1}=l_{x1}+1=3$ $l_{y2}=l_{x2}+1=11$ $l_{y3}=l_{x3}+1=3$		
f_0 (GHz)	**Std**	**Max**	**Std**	**Max**	**Std**	**Max**	**Std**	**Max**	**slope**
2.91	9.55	20.7	0.91	1.92	6.81	14.2	5.68	12.8	P→N
3.86	2.99	4.08	6.88	12	9.16	18.2	5.31	10.9	P→N
4.66	0.04	0.14	0.01	0.02	0.02	0.08	**9.70**	**18.4**	P→N
5.00	0.30	0.82	0.63	1.78	**6.37**	**9.95**	0.14	0.34	P→N
5.08	0.43	2.01	**5.65**	**8.41**	0.19	0.99	0.13	1.14	P→N
5.16	**12.9**	**35.9**	0.89	2.93	0.39	1.23	0.46	1.43	P→N

VI. Reading Range

According to previous calculations [26] by using the Friis formula the reading range for these kind of tags can be up to 3 m with a power level of 0 dBm and a sensitivity of the receiver of -70 dBm. However, it has to be said that mutual coupling between transmitting and receiving ports of the antenna tends to reduce this ideal value [28]. Indeed, when the distance between the reader and the tag is increased, the coupling level between antennas remain at the same level and the signal received back to the tag decreases. The reading range is in our case also limited by the presence of big objects behind the tag. Indeed, as already pointed out, the used time window has to fulfill to two opposite requirements. More in detail, it should be long enough to have a frequency response of the time window at least smaller than the frequency bandwidth of the resonant peaks but, at the same time, it should be short enough to filter out the RCS contributions of the objects close to the tag. In our specific non-anechoic environment case, with a wall at two meters from the tag, the reading range was 50 cm. However, it is not possible to define the reading range independently of the scenario but only an upper bound can be estimated.

VII. CONCLUSION

A novel calibration procedure for chipless RFID is presented and experimentally verified. The encoding/decoding scheme is based on a differential encoding mechanism followed by time domain post processing. The differential encoding is obtained by subtracting the tag response measured simultaneously along two orthogonal planes of incidence. The passive dual polarized tags employed to this purpose comprise an artificial impedance surface able to provide multi-resonant spectral responses. The methodology allows avoiding the usual unpractical calibration procedure thus paving the way to the employment of chipless technology in realistic operative scenarios.

VIII. REFERENCES

[1] R. Das and P. Harrop, "RFID forecasts, players and opportunities 2009–2019," *IdTechEx report*, 2009.

[2] S. Preradovic and N. C. Karmakar, "Chipless RFID: Bar Code of the Future," *IEEE Microw. Mag.*, vol. 11, no. 7, pp. 87–97, Dec. 2010.

[3] V. P. Plessky and L. M. Reindl, "Review on SAW RFID tags," *IEEE Trans. on Ultras., Ferroelectr. Freq. Control*, vol. 57, no. 3, pp. 654–668, Mar. 2010.

[4] S. Gupta, B. Nikfal, and C. Caloz, "Chipless RFID System Based on Group Delay Engineered Dispersive Delay Structures," *IEEE Antennas and Wireless Propag. Lett.*, vol. 10, pp. 1366–1368, 2011.

[5] A. Lazaro, A. Ramos, D. Girbau, and R. Villarino, "Chipless UWB RFID Tag Detection Using Continuous Wavelet Transform," *IEEE Antennas and Wireless Propag. Lett.*, vol. 10, pp. 520–523, 2011.

[6] R. S. Nair, E. Perret, and S. Tedjni, "A temporal multi-frequency encoding technique for chipless RFID based on C-sections," *Progress In Electromagnetics Research B*, vol. 49, pp. 107–127, 2013.

[7] A. Vena, E. Perret, and S. Tedjini, "Chipless RFID Tag Using Hybrid Coding Technique," *IEEE Trans. on Microw. Theory and Tech.*, vol. 59, no. 12, pp. 3356–3364, Dec. 2011.

[8] B. Shao, Q. Chen, Y. Amin, R. Liu, and L.-R. Zheng, "Chipless RFID tags fabricated by fully printing of metallic inks," *Ann. Telecommun.*, vol. 68, no. 7–8, pp. 401–413, Aug. 2013.

[9] F. Costa, S. Genovesi, and A. Monorchio, "A Chipless RFID Based on Multiresonant High-Impedance Surfaces," *IEEE Trans. on Microw. Theory and Tech.*, vol. 61, no. 1, pp. 146–153, Jan. 2013.

[10] S. Preradovic, I. Balbin, N. C. Karmakar, and G. F. Swiegers, "Multiresonator-Based Chipless RFID System for Low-Cost Item Tracking," *IEEE Trans. on Microw. Theory and Tech.*, vol. 57, no. 5, pp. 1411–1419, May 2009.

[11] F. Costa, S. Genovesi, A. Monorchio, and G. Manara, "Calibration method for periodic surface based chipless tags," in *RFID Technology and Applications Conference (RFID-TA)*, 2014, pp. 78–81.

[12] A. Blischak and M. Manteghi, "Embedded Singularity Chipless RFID Tags," *IEEE Trans. on Antennas and Propag.*, vol. 59, no. 11, pp. 3961–3968, Nov. 2011.

[13] V. C. Chen and H. Ling, *Time-frequency transforms for radar imaging and signal analysis*. Artech House, 2001.

[14] J. Li and P. Stoica, "An adaptive filtering approach to spectral estimation and SAR imaging," *IEEE Trans. on Signal Process.*, vol. 44, no. 6, pp. 1469–1484, Jun. 1996.

[15] R. V. De Jough, M. Hajian, and L. P. Ligthart, "Antenna time-domain measurement techniques," *IEEE Antennas Propag. Mag.*, vol. 39, no. 5, pp. 7–11, Oct. 1997.

[16] D. Girbau, J. Lorenzo, A. Lazaro, C. Ferrater, and R. Villarino, "Frequency-Coded Chipless RFID Tag Based on Dual-Band Resonators," *IEEE Antennas and Wireless Propag. Lett.*, vol. 11, pp. 126–128, 2012.

[17] A. Vena, E. Perret, and S. Tedjni, "A Depolarizing Chipless RFID Tag for Robust Detection and Its FCC Compliant UWB Reading System," *IEEE Trans. on Microw. Theory and Tech.*, vol. 61, no. 8, pp. 2982–2994, Aug. 2013.

[18] R. V. Koswatta and N. C. Karmakar, "A Novel Reader Architecture Based on UWB Chirp Signal Interrogation for Multiresonator-Based Chipless RFID Tag Reading," *IEEE Trans. on Microw. Theory and Tech.*, vol. 60, no. 9, pp. 2925–2933, Sep. 2012.

[19] R. Rezaiesarlak and M. Manteghi, "A Space-Frequency Technique for Chipless RFID Tag Localization," *IEEE Trans. on Antennas and Propag.*, vol. 62, no. 11, pp. 5790–5797, Nov. 2014.

[20] R. Mittra, C. H. Chan, and T. Cwik, "Techniques for analyzing frequency selective surfaces-a review," *Proc. IEEE*, vol. 76, no. 12, pp. 1593–1615, Dec. 1988.

[21] F. Costa, S. Genovesi, and A. Monorchio, "On the bandwidth of high-impedance frequency selective surfaces," *IEEE Antennas and Wireless Propag. Lett.*, vol. 8, pp. 1341–1344, 2009.

[22] G. Manara, A. Monorchio, and R. Mittra, "Frequency selective surface design based on genetic algorithm," *Electronics Letters*, vol. 35, no. 17, pp. 1400–1401, 1999.

[23] F. Costa, S. Genovesi, and A. Monorchio, "Chipless RFIDs for Metallic Objects by Using Cross Polarization Encoding," *IEEE Trans. on Antennas and Propag.*, vol. 62, no. 8, pp. 4402–4407, Aug. 2014.

[24] B. A. Munk, *Frequency Selective Surfaces: Theory and Design*. John Wiley & Sons, 2005.

[25] F. Costa, S. Genovesi, A. Monorchio, and G. Manara, "A Robust Differential-Amplitude Codification for Chipless RFID," *IEEE Microw. Compon. Lett.*, accepted for publication 2015.

[26] F. Costa, S. Genovesi, A. Monorchio, and G. Manara, "A circuit-based model for the interpretation of perfect metamaterial absorbers," *IEEE Trans. on Antennas and Propag.*, vol. 61, no. 3, pp. 1201–1209, 2013.

[27] S. Genovesi, F. Costa, A. Monorchio, and G. Manara, "Chipless RFID Tag Exploiting Multifrequency Delta-Phase Quantization Encoding," *IEEE Antennas and Wireless Propag. Lett.*, 2015.

[28] Y. F. Weng, S. W. Cheung, T. I. Yuk, and L. Liu, "Design of Chipless UWB RFID System Using A CPW Multi-Resonator," *IEEE Antennas Propag. Mag.*, vol. 55, no. 1, pp. 13–31, Feb. 2013.

Filippo Costa was born in Pisa, Italy, on October 31, 1980. He received the M.Sc. degree in telecommunication engineering and the Ph.D. degree in applied electromagnetism from the University of Pisa, Pisa, Italy, in 2006 and 2010, respectively. From March to August 2009, he was a Visiting Researcher at the Department of Radio Science and Engineering, Helsinki University of Technology, TKK (now Aalto University), Finland. He is currently an Assistant Professor at the University of Pisa. His research is focused on the analysis and modelling of Frequency Selective Surfaces and Artificial Impedance Surfaces with emphasis to applications in electromagnetic absorbing materials, leaky antennas, radomes, Radio Frequency Identification (RFID), waveguide filters and methods for retrieving dielectric permittivity of materials. He was selected among the ten outstanding reviewers of IEEE Transactions on Antennas and Propagation in 2015. He was recipient of the Young Scientist Award of the URSI International Symposium on Electromagnetic Theory, URSI General Assembly and URSI AT-RASC in 2013, 2014 and 2015, respectively.

Simone Genovesi received the Laurea degree in telecommunication engineering and the Ph.D. degree in information engineering from the University of Pisa, Pisa, Italy, in 2003 and 2007, respectively. Since 2003 he has been collaborating with the Electromagnetic Communication

Laboratory, Pennsylvania State University (Penn State), University Park. From 2004 to 2006 he has been a research associate at the ISTI institute of the National Research Council of Italy (ISTI-CNR) in Pisa. In 2010 he affiliated with the National Laboratory Radar and Surveillance (RaSS). He is currently an Assistant Professor at the Microwave and Radiation Laboratory, University of Pisa. His research is focused on metamaterials, RFID, antenna optimization and evolutionary algorithms.

Agostino Monorchio received the Laurea degree in electronics engineering and the Ph.D. degree in methods and technologies for environmental monitoring from the University of Pisa, Pisa, Italy, in 1991 and 1994, respectively. He is currently an Associate Professor in the School of Engineering, University of Pisa, and Adjunct Professor at the Italian Naval Academy of Livorno. He is also an Adjunct Professor in the Department of Electrical Engineering, Penn State. He is on the Teaching Board of the Ph.D. course in "Remote Sensing" and on the council of the Ph.D. School of Engineering "Leonardo da Vinci" at the University of Pisa.

His research interests include the development of novel numerical and asymptotic methods in applied electromagnetics, both in frequency and time domains, with applications to the design of antennas, microwave systems and RCS calculation, the analysis and design of frequency-selective surfaces and novel materials, and the definition of electromagnetic scattering models from complex objects and random surfaces for remote sensing applications. He has been a reviewer for many scientific journals and he has been supervising various research projects related to applied electromagnetic, commissioned and supported by national companies and public institutions.

Dr. Monorchio is IEEE Fellow. He has served as Associate Editor of the IEEE ANTENNAS AND WIRELESS PROPAGATION LETTERS. He received a Summa Foundation Fellowship and a NATO Senior Fellowship.